Journal of Applied Mechanics Vol. 5, pp. 629-638 (August 2002) JSCE

Numerical Simulation of Bar Formation in Straight Channels by the NHSED2D Model

NHSED2D モデルを用いた直線河道の砂州形成数値シミュレーション

Adichai PORNPROMMIN*, Atsuko TERAMOTO*, Norihiro IZUMI**
Tadanori KITAMURA***, Tetsuro TSUJIMOTO****
アディチャイ ポンプロミン，寺本敦子，泉 典洋，北村忠紀，辻本哲郎

* M. Eng., Doctoral Student, Dept. of Geo-tech. & Env. Eng., Nagoya University
(Furo-cho, Chikusa-ku, Nagoya 464-8603, Japan)
** Ph.D., Associate Professor, Dept. of Civil Eng., Tohoku University
*** Dr. Eng., Div. of Environment and Water Resources, Pacific Consultants International
**** Dr. Eng., Professor, Dept. of Geo-tech. & Env. Eng., Nagoya University

Numerical simulations are performed to investigate the characteristics of the formation of alternate and multiple bars with the use of the NHSED2D model. The results of the simulations show reasonably good agreement with the results of the theoretical analysis and the experiments. It is found that periodic boundary conditions with an insufficiently small calculation domain tend to stabilize multiple bars. It is also found that there is possibility that different initial configurations lead to different equilibrium states. The reduction of the bar mode can be well explained by the theoretical results that the difference between the dominant modes associated with the maximum growth rate and the maximum equilibrium amplitude. The irregularity appeared in the reduction process of the bar mode is suggested to be caused by the nonlinear interaction between multiple modes of bars.

Key Words: bar formation, alternate bar, multiple bar, numerical simulation

1. Introduction

The interaction between flow and its boundaries provides a variety of riverbed patterns. The instability of erodible beds leads to the formation of bars, which are categorized by the bar mode n, the number of bars laterally contained in the channel, into single alternate bars and multiple bars as shown in Fig. 1.

Bar formation in rivers has been one of the greatest concerns for many river engineers and researchers because it plays significant roles in both engineering and ecological aspects in fluvial processes. For instance, pools caused by bar formation as shown in Fig. 1 induce successive side bank erosion while sandbars are habitats for various species in rivers.

A large number of studies have been conducted on the bar formation. Only a brief review of the studies related to this paper is provided herein. Ikeda[1] proposed empirical formulas to predict the wavelength and wave height of alternate bars. He tested his formulas by a number of experimental data obtained by himself and other researchers. Fujita[2),3)] performed numerous experiments to investigate the formation processes of alternate and multiple bars, and braided streams. He found that in most of the cases, the bar mode is reduced as time progresses.

Theoretical studies started with linear stability analysis[4),5),6),7)], which successfully described the regime of bar formation. However, the linear theories can describe only the very beginning of bar formation. When the amplitude grows to be finite, the linear theory is invalid because of the domination of nonlinear terms.

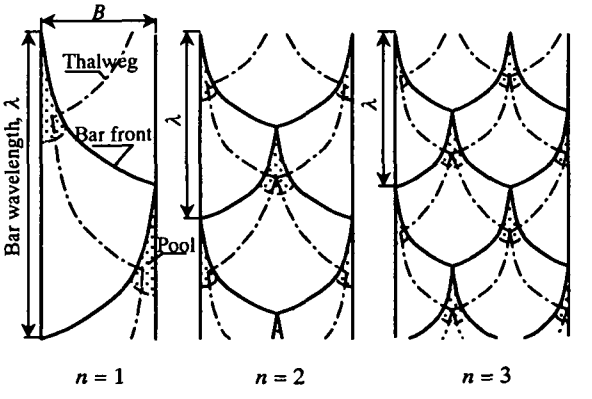

Fig.1 Alternate bar (left) and multiple bars (middle and right).

Nonlinear stability analyses have been conducted in the last few decades. Fukuoka & Yamasaka[8] performed a nonlinear analysis assuming the interaction between two different modes of bars to treat equilibrium states. Colombini *et al.*[9] proposed a nonlinear stability analysis by the growth rate expansion method to obtain the wave height of alternate bars. Two of the authors of this paper proposed another nonlinear analysis[10),11)] to extend Colombini *et al.*'s to more general cases. In order to remove the restriction of small growth rates, the amplitude expansion method was used to derive the equilibrium wave height of both alternate and multiple bars.

In recent years, numerical models of bar formation have been developed thanks to the rapid development of computers. Egashira & Takebayashi[12], and Takebayashi *et al.*[13] performed numerical simulations of bar formation, and succeeded in reproducing the reduction of bar mode as observed in Fujita's experiments. Kurabayashi *et al.*[14] and Kurabayashi & Shimizu[15] proposed another numerical simulation model using the CIP method that minimizes the numerical diffusion. Their model also succeeded in reproducing the transition from multiple bars to braided streams.

In the study presented herein, the Nagoya Hydraulics Surface and Subsurface 2-Dimensional simulation model (NHSED2D) is used to investigate the formation processes of alternate and multiple bars in more detail. The simulation results are compared with both theoretical results[10), 11)] and experimental data[2), 3)] in order to clarify the effects of initial and boundary conditions on the bar formation process. The cause of the reduction of bar mode observed in experiments is also discussed in terms of the theoretical and numerical analyses.

2. NHSED2D model formulation

The NHSED2D model comprises two main parts, the flow model and the sediment transport & bed variation model. At first, the flow is computed over an initial bed configuration until it converges. Then, the sediment transport and the resultant bed variation are calculated using the flow field. After the bed is renewed, the flow is calculated again on the renewed bed. These procedures are repeated to obtain successive bed deformation. The NHSED2D model is essentially based on the model developed by Tsujimoto *et al.*'s[16]. The model is modified to include semi-coupling of surface and subsurface flow and the periodic boundary condition for the simulation of bar formation in this study.

2.1 Flow model

The 2D depth-averaged flow model has the following significant features:

- The finite volume method is employed to discretize the governing equations.
- The fractional step method to solve the Poisson equation of water surface elevation is employed in order to obtain the stable and accurate flow field[17].
- To prevent numerical oscillation due to collocated grid arrangement, the idea according to Rhie and Chow[18] to interpolate the flux of mass at the cell surface is used.
- The QUICK scheme is employed for interpolating the convection of momentum at the cell surface.
- Semi-coupling of surface and subsurface flow is used in the region where emerged bars appear.
- Periodic boundary conditions are employed for both flow and sediment transport.

The governing equations of 2D depth-averaged surface flow can be described by the following equations:

$$\frac{\partial q_x}{\partial t}+\mathrm{div}\left(q_x\frac{\mathbf{q}}{h}-\frac{\mathbf{T}_x}{\rho}\right)=-gh\frac{\partial \zeta}{\partial x}-\frac{C_f}{h^2}q_x|\mathbf{q}| \qquad (1)$$

$$\frac{\partial q_y}{\partial t}+\mathrm{div}\left(q_y\frac{\mathbf{q}}{h}-\frac{\mathbf{T}_y}{\rho}\right)=-gh\frac{\partial \zeta}{\partial y}-\frac{C_f}{h^2}q_y|\mathbf{q}| \qquad (2)$$

$$\frac{\partial \zeta}{\partial t}+\mathrm{div}\mathbf{q}=0 \qquad (3)$$

where t is time, x and y are the streamwise and lateral coordinates respectively, q_x and q_y are the x and y components of the discharge flux, $\mathbf{q}$ is the discharge flux, ζ is the water surface elevation, h is the flow depth, $\mathbf{T}_x$ and $\mathbf{T}_y$ are the x and y components of the Reynolds stress tensor, g is the gravity acceleration, and C_f is the resistance coefficient of bed surface. The kinematic-eddy viscosity is assumed to be proportional to the shear velocity and depth.

When the flow depth h is less than critical value ($= 2D_s$, where D_s is the sediment diameter), the following governing equations for subsurface flow are solved instead of Eqs. (1) – (3):

$$\frac{\partial \zeta}{\partial t}+\mathrm{div}\left(C_{sub}\,\mathrm{grad}\zeta\right)=0 \qquad (4)$$

$$C_{sub}=\frac{K(\zeta-z_{sub})}{n_e} \qquad (5)$$

where K is the permeability of the subsurface layer, z_{sub} is the elevation of the bottom of subsurface layer, and n_e is the porosity of subsurface layer. We assumed z_{sub} is a constant of 0.5 m below the bed elevation for simplicity. However, this does not affect on the bar formation process as far as emerged bars are not so large.

When an emerged bar appears at a node, additional conditions are required between the node and the adjacent nodes. Proper treatment of the water surface gradients around the node is necessary. This significance is also mentioned by Kurabayashi & Shimizu[15]. In our model, the appropriate water surface gradient can be computed with the use of the semi-coupling of surface and subsurface flow expressed as Eqs. (4) and (5) in a physically rational manner.

2.2 Sediment and bed variation models

The time variation of the bed elevation can be described by the following sediment continuity equation:

$$(1-n_e)\frac{\partial z}{\partial t}=-div\mathbf{q}_b \qquad (6)$$

where z is the bed elevation, and $\mathbf{q}_b$ is the sediment flux vector, which is estimated by the Ashida & Michiue formula[19]. The x and y components of the sediment flux (q_{Bx}, q_{By}) are estimated by the following equations:

$$q_{Bx}=q_B\cos\varphi,\quad q_{By}=q_B\sin\varphi \qquad (7a, 7b)$$

where q_B is the total bedload transport rate per unit width, and φ is the angle of bedload movement.

The effect of transverse bed slope on the sediment transport is taken into account following Nakagawa *et al*[20]. The model also includes the effect of secondary flow caused by the curvature of streamlines using Engelund's equation[21]. The angle of bedload movement φ is expressed by the following equation:

$$\varphi=\tan^{-1}\left(\frac{V}{U}-N_*\frac{h}{r}\right)-\tan^{-1}\left(\sqrt{\frac{\tau_{*c}}{\mu_d\mu_f\tau_*}}\frac{\partial z}{\partial n}\right) \qquad (8)$$

where U and V are the velocity components in the x and y directions respectively, N_* is the coefficient of the strength of secondary flow (=7.0 as given by Engelund), r is the curvature radius of a streamline, μ_f and μ_d is the static and kinetic friction coefficients of sand grains respectively, τ_* is the Shields number, τ_{*c} is the critical Shields number, and n is the coordinate normal to a streamline.

After calculating bed variation, the bed slope angles $\tan^{-1}(\partial z/\partial x)$ and $\tan^{-1}(\partial z/\partial y)$ between adjacent grids on the bed are compared with the angle of repose ϕ. In the case that the bed slope angle is greater than the angle of repose ϕ, the bed is assumed to collapse with the angle ϕ.

After iterating the flow calculation *noflowitr* times in order for the flow to reach a quasi-steady condition, the sediment and bed variation are computed as conceptualized in Fig. 2. While the time step of flow calculation Δt remains constant, the time step of sediment computation Δt_s, which is the controlling time for the simulation is adjusted by ε as described in Eq. (9). We found that ε should be around $0.004D_s$ to obtain numerical stability.

$$\Delta t_s = \frac{\varepsilon}{\left|\frac{\partial z}{\partial t}\right|_{\max}} \tag{9}$$

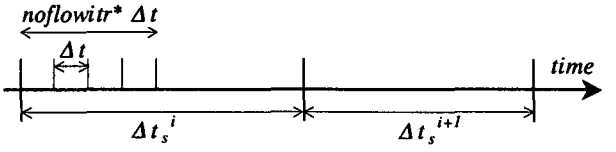

Fig.2 The conceptual sketch of flow and sediment time steps.

2.3 The initial and boundary conditions

There are two possible approaches to specify the initial and boundary conditions for the simulation of bar formation in which instability needs to be induced. One is to use the periodic boundary conditions in the calculation domain. Small disturbances are given to the initial flat bed to achieve instability. The other approach is to give disturbances only to the upstream boundary; all the other initial variables are undisturbed. While the influence of the initial disturbance is reduced after sufficiently long time in the former approach, it remains persistently in the upper reach of the calculation domain in the latter case. Considerably long domain is necessary to achieve self-organized bed configuration, resulting in long calculation time in the second approach. Although the latter approach is more equivalent to most of experiments, the periodic boundary condition is employed because of the limitation of CPU performance in this study. The domain length selected in this approach requires great scrutiny because it is expected to have strong influences on the results, which is to be revealed later in the present study.

3. The simulation of alternate bars

In this section, we attempt the simulation of the formation of alternate bars. The results are compared with the corresponding experimental and theoretical results.

3.1 Description on the experimental study

The formulation described in the previous section is applied to the case of alternate bars (n = 1). Some qualitative characteristics of alternate bars observed in experiments are described in the following[2]:

- Immediately after the flow commencement, sand grains are swept straight downstream, with fluctuating left and right to some extent.
- After a while, obliquely directed lines with very small height appeared here and there on the bed.
- The sand grains seem to be trapped on and under the lines, which become small steps with increasing height.
- Some of them are seen to turn into clearly distinguished bar edges, increasing their height.
- These bar edges continue to develop till they reach an equilibrium state.
- Longitudinally averaged cross-sections of the bed are characterized by Quonset hut-shaped (bell-shaped) configurations.

The model is tested using Fujita's Run C-2 described in table 1, in which the aspect ratio β is the ratio between channel width and flow depth. The aspect ratio is an important parameter, which determines the bar mode n, when larger β generally corresponds to larger n.

Table 1 Experimental data of Fujita's Run C-2.

Run no.	C-2
Channel width B (m) x length L (m)	0.40 x 18
Water discharge Q (l/s)	1.95
Slope S	0.01
Sediment Diameter D_s (mm)	0.99
Water Depth H (mm)	12.6
Aspect ratio β	31

3.2 Conditions of the numerical simulation

Conditions employed in the simulation are described in table 2, in which Z_0 is the initial bed elevation, ε is the control parameter to determine the time step for sediment transport and bed deformation as already described, and "Nran" means the disturbance with a normal distribution, which has a mean value of zero and a standard deviation of 0.1. We adopt normally distributed random disturbances that are considered to reproduce experimental situation appropriately. The application of the disturbance with a normal distribution have been employed in other studies such as Dey *el at.*'s[22]. The length of the calculation domain is taken to be 3 m which corresponds to the bar wavelength observed in the experiment.

Table 2 Conditions of the simulation for Fujita's Run C-2.

Domain B (m) x L (m)	0.40 x 3
No. of nodes (Lateral x Streamwise)	16 x 40
Δt (s)	0.01
Z_0 type	Nran
ε	$0.004D_s$
Total time (min)	140

3.3 Results of the simulation for Fujita's Run C-2

Fig. 3 shows the bed variation in each time step obtained in the simulation. At the beginning of the simulation, the small random disturbances set to be the initial bed. It is found that the disturbances evolve into alternate bars, and that the bar height increases with time. After about 1 hour, the alternate bar reaches an equilibrium state to become fully developed alternate bars, propagating downstream with a stable regular shape.

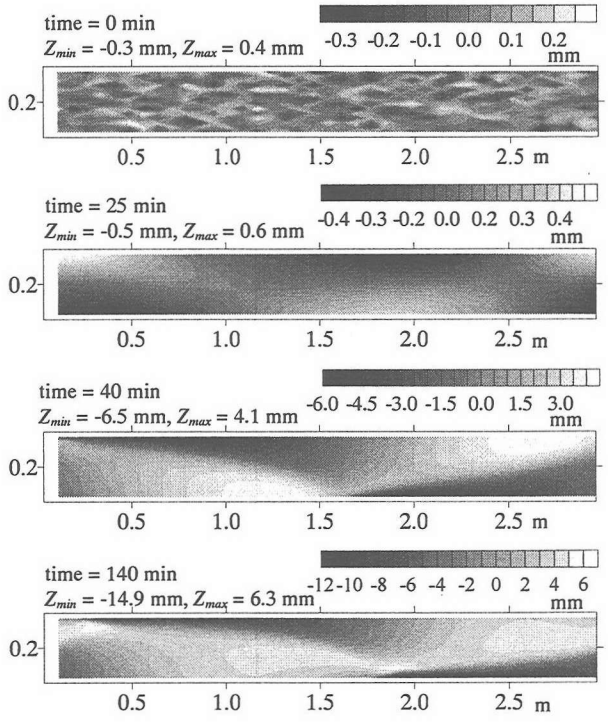

Fig.3 Bed topography of the simulation for Fujita's Run C-2.

3.4 Discussion on the simulation of alternate bars

In Fig. 4, the results of the simulation are compared with those of the theoretical analysis performed by two of the authors (the detailed description of the theory is not provided herein due to the limitation of space. See the references 10 and 11). The bar height observed in the experiment is 25.8 mm and that derived from theory is 29.5 mm while the numerical simulation gives a smaller value of 21.1 mm. The bar height, which is defined as the difference between the maximum and minimum bed elevations in one wavelength, is overestimated in the theory. This is because the bar shape is represented by only three different Fourier modes in the theory, in which local scour and deposition are too exaggerated. Nevertheless the agreement of water surface elevation and bed topography is reasonably good. Fig. 5 shows the bed topography derived from the theory. Compared with Fig. 3, the numerical simulation is found to give more realistic topography than the theory does.

Longitudinally averaged cross-sections derived from the numerical simulations are compared with the experimental result in Fig. 6. It is found that the cross-section is characterized by the bell-shaped configuration, which is well reproduced by the numerical simulation. Though the agreement between the experimental result

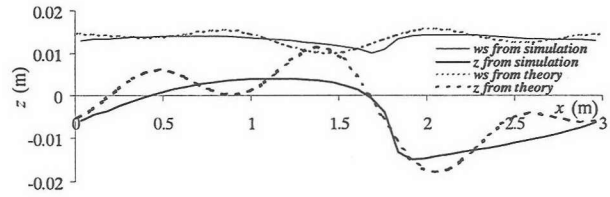

Fig.4 Comparison of longitudinal profiles of Fujita's Run C-2 at y = 0.0125 m between the numerical simulation and theory. *ws* denotes the water surface elevation.

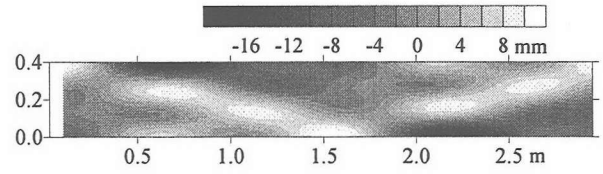

Fig.5 Bed topography of Fujita's Run C-2 derived from the theory.

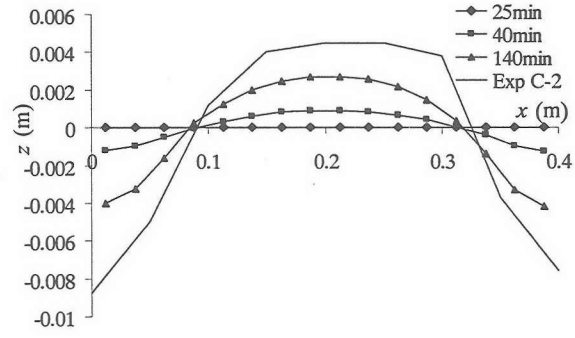

Fig.6 The longitudinally averaged cross-sections of Fujita's Run C-2. Lines with symbols are numerical results, and only line is the experimental results.

and the simulated result in equilibrium (t = 140 min) is reasonably good, the vertical scale of the simulated result is not sufficiently large. There is a possibility that this discrepancy is caused by the fact that the secondary flow is not well reproduced in the present model[23].

4. The simulation of multiple bars

In this section, the simulations of multiple bars are performed and the results are compared with Fujita's experimental data[3]. The aspect ratio β is set to be higher than that in the simulation of alternate bars, implying shallower water channels. Four cases with different initial conditions and domain lengths are studied in order to clarify the influence of the initial and boundary conditions on the bar formation process, and to discuss the mechanisms of the reduction of bar modes and the transition to braided channels in terms of the numerical simulation, theory and experiments.

4.1 Description on the experimental study

In the case of multiple bars, the situations are more complicated since it is known that multiple bars are unstable to evolve into a braided configuration. Significant characteristics of multiple bars[3] observed in Fujita's experiments are summarized in the following:

- It is observed in some cases, that regular, symmetrical high modal bars appear on the early stage, and that they merge together to evolve into lower modal bars.
- In the transition to lower modal bars, sudden changes of bar geometry, increase in wavelength and heights, lead the appearance of braided patterns in some cases.
- The cross-sectional shapes averaged longitudinally are different in each sub-reach. This suggests a spatial change in the mechanism of bed evolution even in the case without emerged bars.
- The bed change is more rapid in the experimental cases with steeper slopes.

The model is tested using Fujita's Runs B-2 and B-4, the conditions of which are shown in table 3.

Table 3 Hydraulic conditions of Fujita's Runs B-2 and B-4.

Run	B-2, B-4
Channel width B (m) x length L (m)	3.01 x 43
Water discharge Q (l/s)	30.75
Slope S	0.005
Sediment Diameter D_s (mm)	0.88
Water Depth H (mm)	25.5
Aspect ratio β	124

The Runs B-2 and B-4 are conducted under the same hydraulic conditions. The only difference is the fact that in the Run B-4, the experiment was interrupted six times to measure the bed topography. Table 4 provides the description of both experiments, and Figs. 7 and 8 show the bed topographical changes observed in the Runs B-2 and B-4, respectively. In table 4, λ_{exp} and Z_{Bexp} are the wavelength and wave height of bars observed in the experiments.

Table 4 Description of the results of the Runs B-2 and B-4.

Time	N	λ_{exp} (m)	Z_{Bexp} (mm)	Description
B-2				
0'				Helicoidal flow with longitudal streaks
15'				Small water surface wave at upstream. Below it, a feature like a bar edge migrates downstream.
3hr39'	2	13	~80	A symmetrical form
B-4				
0'	~4			Helicoidal flow, water surface wave, very thin bar of mode ~4 at early interruption.
2hr33'	4	~5	~40	Mode 4 was not found in B-2.
4hr15'	2	~13	~90	Bar wavelength & height increase, n decreases.
Final	~1.5			Irregular bars, some emerged, and single meandering thread.

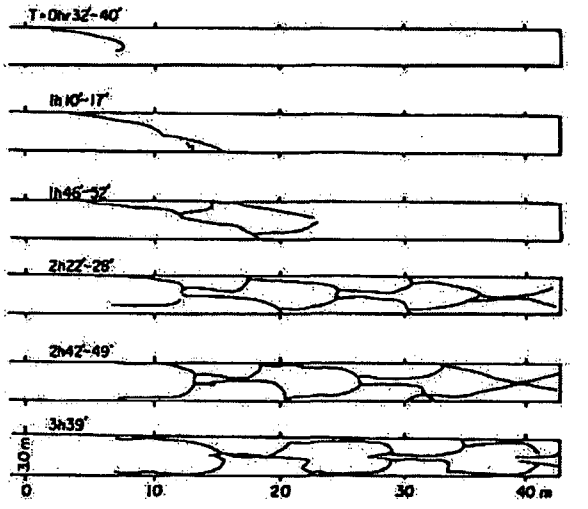

Fig.7 The bed topographical change observed in the Run B-2.

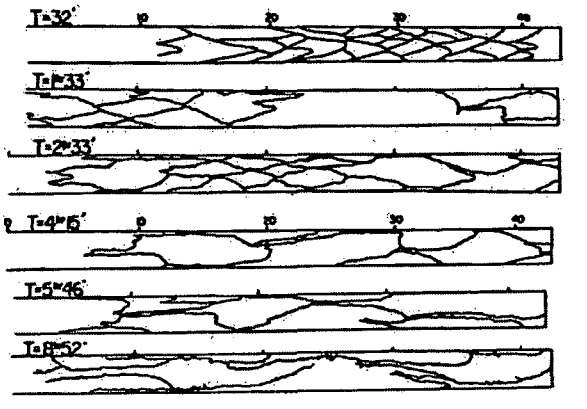

Fig.8 The bed topographical change observed in the Run B-4.

4.2 Conditions of the numerical simulation

Since the periodic boundary condition is assumed to have a strong influence on the bar wavelength, several different domain lengths are used in the simulations. The different initial conditions are also employed to clarify the influence. The conditions used in the four simulations are described in Table 5.

As described earlier, the periodic boundary condition does not represent the experimental condition, when the domain length is expected to be of great importance. We employed three different domain lengths in order to clarify the significance of the length in the case of the periodic boundary condition.

Table 5 Conditions of the simulations for Fujita's Runs B-2 and B-4. "Sine" means that Z_0 is set to be a sinusoidal shape.

Simulation No.	1	2	3	4
B (m) x L (m)	3.01 x 5		3.01 x 15	3.01 x 25
No. of nodes	30 x 50		30 x 75	30 x 100
Δt (s)	0.01		0.02	0.03
Z_0 type	Sine	Nran	Nran	Nran
ε	$0.004D_s$			
Total time (hrs)	4.5	5.0	7.0	5.1

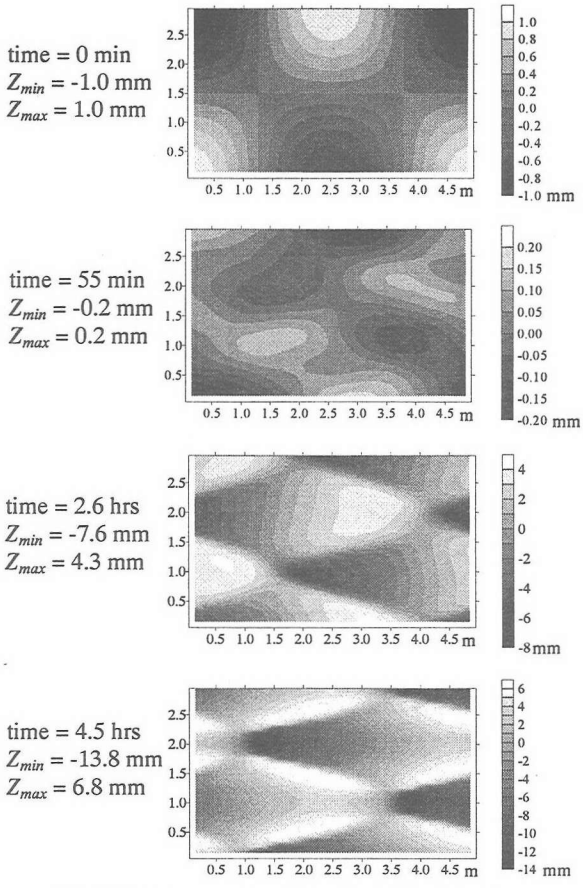

Fig.9 Bed topography of the simulation No. 1.

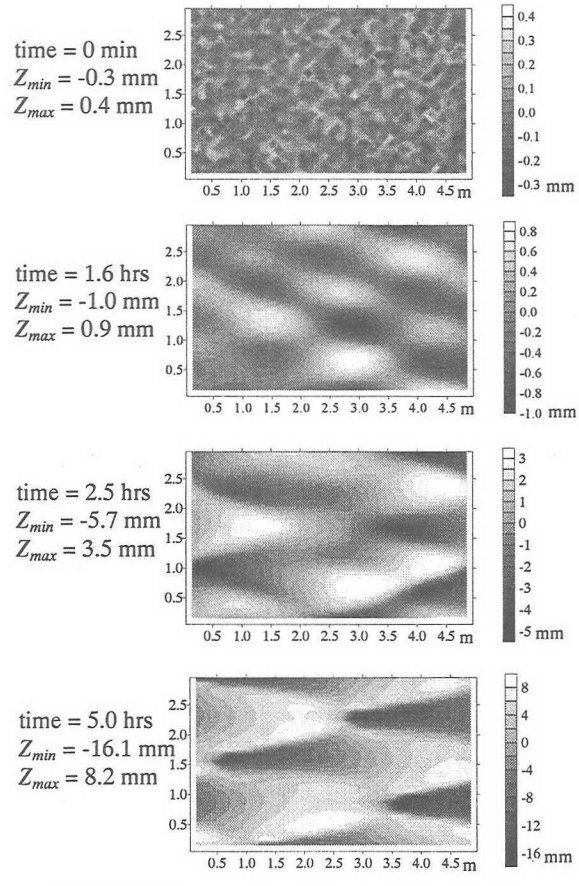

Fig.10 Bed topography of the simulation No. 2.

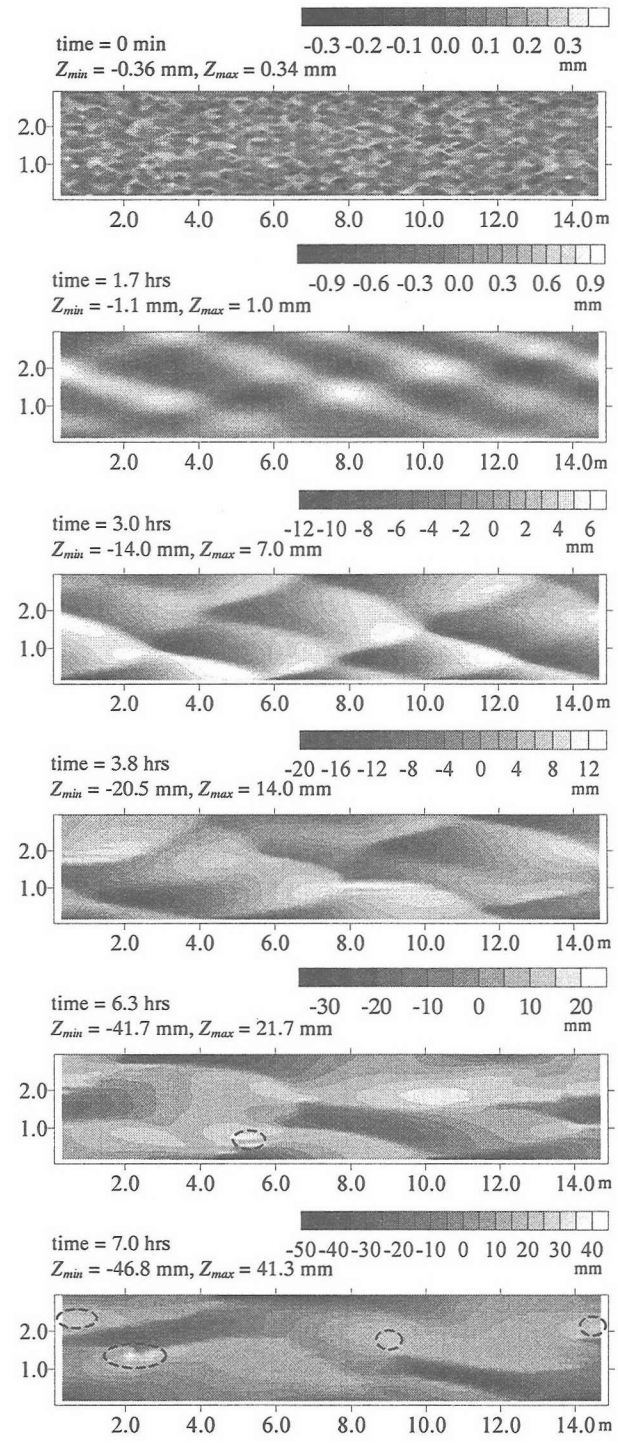

Fig.11 Bed topography of the simulation No. 3. Emerged bars are indicated by broken circles.

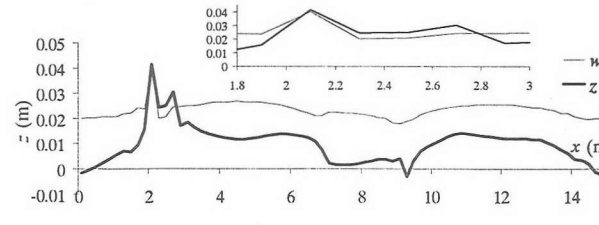

Fig.12 The longitudinal profile of the simulation No. 3 at y = 1.35 m. The small figure shows the vicinity of the emerged bar.

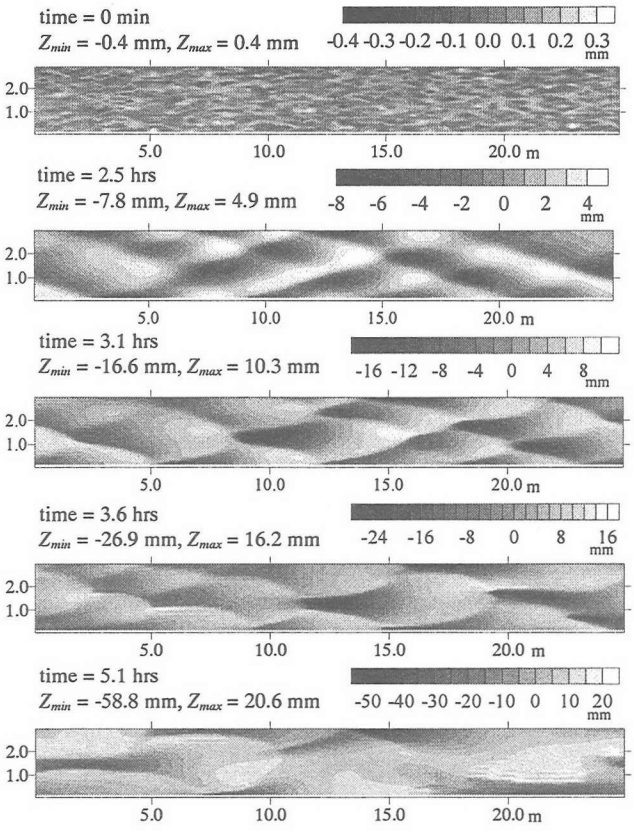

Fig.13 Bed topography of the simulation No. 4.

4.3 Results of the simulations for Fujita's Runs B-2 and B-4

(1) The simulation No. 1

It is found that, at the beginning, the initial sinusoidal bed topography with the mode $n = 1$ evolves into the bars with the mode $n = 3$ as shown in Fig. 9. The bar height increases with the evolution of the mode. In the final stage, a stable symmetrical form of multiple bars with the mode $n = 3$ is observed, the wavelength of which is equivalent to the domain length. Therefore, it implies that alternate bars ($n = 1$) with the wavelength equal or less than 5 m cannot appear in the simulation.

(2) The simulation No. 2

Fig. 10 shows the formation process of the simulation No. 2. The disturbances with a normal distribution are given on the surface as an initial condition. While the mode $n = 5$ with the wavelength around 3 m, is dominantly observed at the beginning, it is reduced to the mode $n = 4$. The bar height increases with reducing mode. Symmetrical bars with the mode $n = 4$ become dominant in equilibrium. It is interesting that although all the conditions other than the initial condition are identical between both simulations No. 1 and 2, the final bar modes are different from each other. This implies that there are two different equilibrium solutions in this case.

(3) The simulation No. 3

In this case, the domain length is extended to be 15 m. The initial condition is small random disturbances with a normal distribution. The time variation of the bed topography is shown in Fig. 11. At the beginning, the small disturbances decay rapidly, and bars with the mode $n = 3 \sim 4$ appear. Then, the bars with the mode $n = 3$ become dominant in the whole region. The bar height and the wavelength increase with reducing bar mode from $n = 3$ to 2. The bars with the mode $n = 2$ are rather irregular and an emerged bar appears at 6.3 hrs. The bed configuration is similar to alternate bars though the bar pattern is rather irregular and emerged bars increasingly appear as time progresses. The longitudinal bed profile at $t = 7.0$ hrs that emerged bars already appeared in the simulation along $y = 1.35$ m is shown in Fig. 12.

(4) The simulation No. 4

This simulation is conducted in the longest simulation domain. Rather symmetrical bars with the mode $n = 3$ are found at the beginning as shown in Fig. 13. The bars migrate downstream and increase their height. The merging process of bars from the mode $n = 3$ to $n = 2$ is clearly observed in some regions. The wavelength increases with decreasing bar mode. In this case, the symmetrical bars with the mode $n = 2$ and a wavelength of about 8 m are found in the figure. It is found that the bed evolution processes seen in the simulations No. 3 and 4 are rather similar to each other; the bar mode $n = 3$ is dominant first, and is reduced to the mode $n = 2$. The irregularity increases with decreasing mode.

4.4 Discussion on the simulations for multiple bars

(1) The effects of initial and boundary conditions

In each simulation, the process of bed evolution is found to be rather different. This is caused by the influence of the domain length and the initial conditions. In the simulations No. 1 and 2, the stable patterns of multiple bars appear. The bar wavelength λ is forced to be equivalent to the domain length by the periodic boundary conditions because the domain is not long enough. It is suggested that the large effect of the boundary condition seems to stabilize multiple bars. In addition, these two cases end up with different final patterns; two different initial conditions result in two different final configurations. These results suggest that there exist at least two equilibria that are induced by different initial conditions in this case.

It is found that boundary conditions are essential to solutions (bar modes) that can exist in a channel. This further suggests that solutions or bed configurations are strongly influenced by the change of boundary conditions such as riverbank erosion or the formation of emerged bars.

(2) The modal transition (reduction)

The results compared with the theoretical analysis provide a useful insight on the bar formation. The characteristic wavelength associated with the maximum growth rate is commonly assumed to be the dominant wavelength that appears in the field. Fig. 14 shows the relation between the growth rate and wavelength λ for each mode. For $\lambda = 5$ m, the theory shows that the bars with the mode $n \geq 2$ can develop. This corresponds to the simulation No. 1, where the initial bar mode $n = 1$ changes into $n = 3$ because the domain length is 5 m. We have tried starting with a sinusoidal shape with the mode $n = 2$, and have found the initial mode ($n = 2$) was stable,

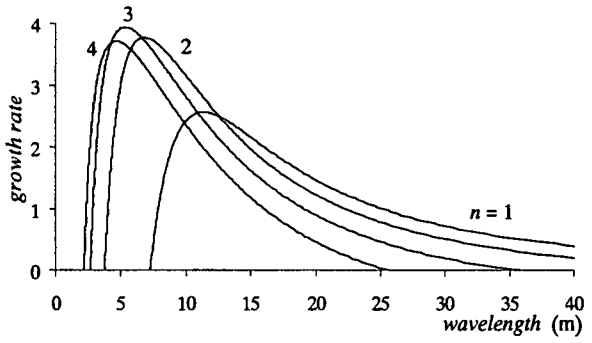

Fig.14 The linear growth rate as a function of the wavelength and the mode n derived from the theory.

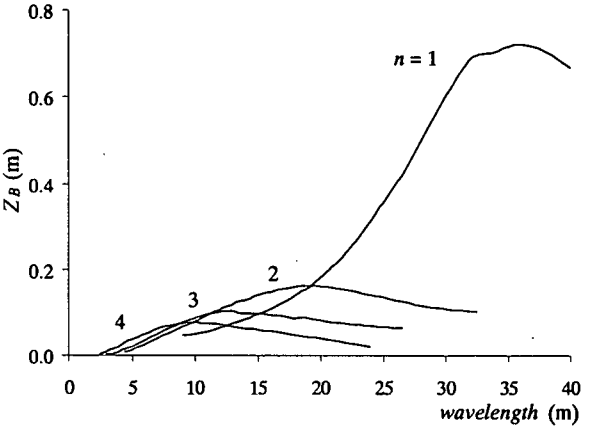

Fig.15 Bar height Z_B as a function of the wavelength and the mode n derived from the theory.

though the results are not shown herein because of the limitation of space.

The domain lengths of the simulations No. 3 and 4 are 15 and 25 m, respectively. It is found in Figs. 11 and 13 that the bars with the mode n = 3 and the wavelength λ = 4-6 m firstly appear. According to the theoretical results shown in Fig. 14, the bars with the mode n = 3 have a higher growth rate than those with the other modes, and that the maximum growth rate corresponds to a wavelength around 5 m.

The relation between the bar height Z_B and the wavelength λ for several modes derived from the theory is shown in Fig. 15. From the figure, the bar height Z_B corresponding to the modes n = 3 and 4 are found to be 28 mm and 36 mm, respectively, when the wavelength λ is 5 m. In the simulations No. 1 and 2 in which the modes n = 3 and 4 appear, respectively, and the wavelength is constrained to be 5 m by the domain length, the bar heights Z_B are 20 and 24 mm, respectively. Meanwhile, bars with n = 4, Z_B = 40 mm, and λ = 5 m were observed in Fujita's experiment (Run B-4 at t = 2hrs 33min). This suggests that the mode with the larger bar height becomes dominant in reality. In addition, the qualitative agreement is found to be good among the simulation, experiment and theory though the quantitative agreement is not prefect.

It is found, in Figs. 14 and 15, that the wavelength associated with the maximum bar height Z_B is far larger

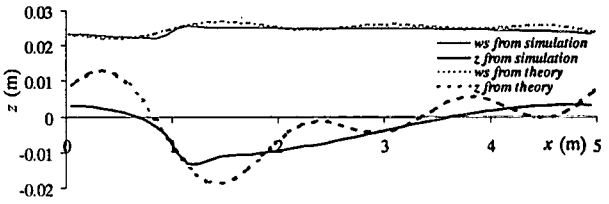

Fig.16 The comparison of the longitudinal profile in the simulation No. 1 at y = 0.05 m, t = 4.5 hrs with the corresponding theoretical result. Solid and broken lines indicate the simulated and theoretical results, respectively, and ws denotes the water surface elevation.

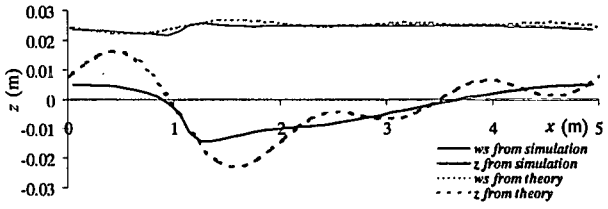

Fig.17 The comparison of the longitudinal profile in the simulation No. 2 at y = 0.05 m, t = 5.0 hrs with the corresponding theoretical result.

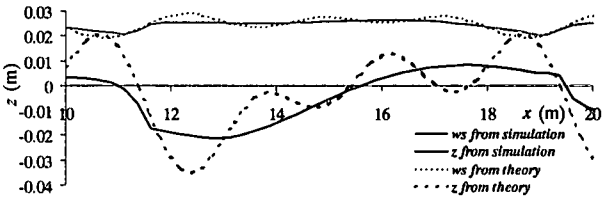

Fig.18 The comparison of the longitudinal profile of the simulation No. 4 from x = 10 to 20 m at y = 1.5 m and t = 3.6 hrs with the corresponding theoretical result.

compared with the characteristic wavelength defined by the maximum growth rate. Fig. 15 also shows that the lower modes give the larger maximum bar height Z_B. This causes the fact that higher modal multiple bars with shorter wavelength tend to merge each other and evolve into lower modal bars with larger bar height.

We saw an example in which two different equilibria were induced by two different initial bed conditions even under a rather strict boundary condition. In the case of natural channels with a large aspect ratio, various modes of bars can develop in the channel because the effect of boundary condition is so small. The questions as to which mode dominantly appears or how the modal reduction occurs can be generally answered by the theory as discussed above. This process is not so simple however. The irregularity that appeared in the reduction process of the bar mode suggests the nonlinear interaction between multiple modes of bars. The nonlinear interaction may be an essential factor to cause the strong irregularity and instability of braided streams.

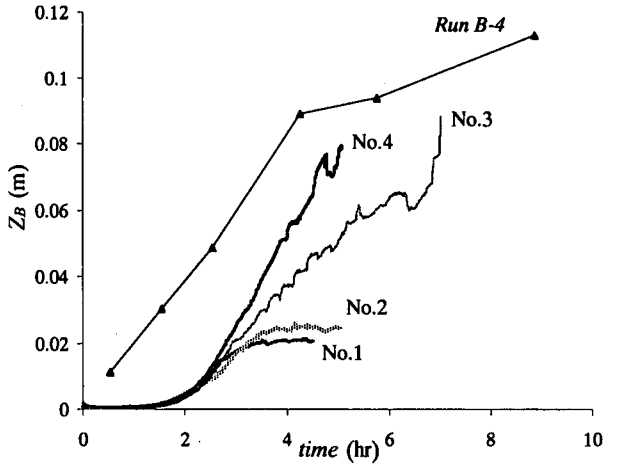

Fig.19 The time development of bar height of the simulation No. 1-4 compared with the results of the Run B-4.

(3) Longitudinal profiles, time development of bar height and longitudinally averaged cross-sections

Figs. 16, 17 and 18 show the comparison of the longitudinal profiles in the simulations No. 1, 2 and 4 with the corresponding theoretical results, where the bar modes are found to be n = 3, 4 and 2, respectively. The agreement between the numerical simulations and the theory is reasonably good. The high bed elevation occurs because of the exaggeration of insufficient number of the Fourier mode included in the theoretical solution in that particular case. It is expected that, if more Fourier modes are included, the exaggeration is attenuated. Nevertheless, the theory is applied to the case beyond its applicability, and show good agreement in the nonlinear analysis performed by two of the authors. In a similar manner, though the theory is not applicable to the emerged bars in fact, it provides good agreement even in the range beyond its applicability.

The time development of the bar height Z_B in each simulation is shown in Fig. 19. The figure shows that the bar height cannot grow in the case to the simulation No. 1 and 2. This implies that the insufficient domain length of simulation No. 1 and 2 only allows for the appearance of higher modal bars with small bar height. Though the time development of bar height simulated by the numerical model is generally slower at the beginning, the agreement is improved afterwards. This is probably caused by the difference of the magnitude of initial disturbance.

The longitudinally averaged cross-sections of the simulation No. 2, 3 and 4 are shown in Figs. 20, 21 and 22, respectively. Compared with the results of the Run B-2, the best agreement is found in the case of the simulation No. 4, which employs the longest calculation domain in the four cases. This implies the longitudinally averaged cross-section is also strongly influenced by the domain length.

5. Conclusions

Numerical simulations are performed to study bar formation in straight channels with the use of the

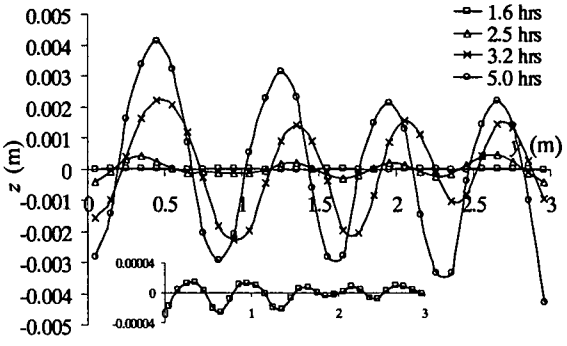

Fig.20 The time development of longitudinally averaged cross-sections of the simulation No. 2. The vertical scale at t = 1.6 hrs is enlarged in the small figure.

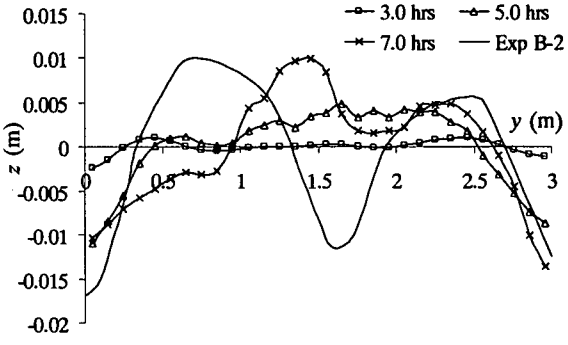

Fig.21 The time development of longitudinally averaged cross-sections of the simulation No. 3 compared with the experimental results.

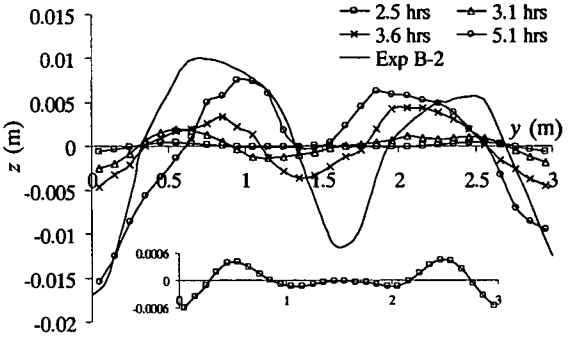

Fig.22 The time development of longitudinally averaged cross-sections of the simulation No. 4 compared with the experimental results. The vertical scale at t = 2.5 hrs is enlarged in the small figure.

NHSED2D. The results of the simulations show reasonably good agreement with the theoretical and experimental results. It is found that different initial conditions lead to different equilibrium states. It is also found that initial and boundary conditions have strong influences on bar modes that appear in channels. The process of modal reduction can generally explained by the theory. However, the irregularity appeared in the reduction process of the bar mode is suggested to be caused by the nonlinear interaction between multiple modes of bars. This process is far more complicated.

Acknowledgement

The authors are grateful to Prof. Fujita, Gifu University, for kindly providing his papers.

References

1) Ikeda, S., Prediction of alternate bar wavelength and height, *J. Hydr. Eng.* **110(4)**, pp.371-386, 1982.
2) Fujita, Y. and Muramoto, Y., Studies on the process of development of alternate bars, *Bulletin of the disaster prevention research institute* **35**, Kyoto, pp.55-86, 1985.
3) Fujita, Y., Bar and channel formation in braided streams, *River meandering*, Water Resources Monograph **12**, pp.417-462, 1989.
4) Hansen, E., The formation of meanders as a stability problem, *Hydraul. Lab., Tech. Univ. Denmark Basic Res. Prog. Rep.* **13**, 1967.
5) Engelund, F. and Skovgaard, O., On the origin of meander-ing and braiding in alluvial streams, *J. Fluid Mech.* **57**, pp.289-302, 1973.
6) Parker, G., On the cause and characteristic scales of meandering and braiding in rivers, *J. Fluid Mech.* **76(3)**, pp.457-480, 1975.
7) Fredsøe, J., Meandering and braiding of rivers, *J. Fluid Mech.* **84(4)**, pp.609-624, 1978.
8) Fukuoka, S. and Yamasaka, M., Equilibrium height of alternate bars based on non-linear relationships among bed profile, flow and sediment discharge, *Hydraul. and Sanitary Eng.* **357(II-3)**, Proceedings of JSCE, pp.45-54, 1973. (in Japanese)
9) Colombini, M., Seminara, G. and Tubino, M., Finite amplitude alternate bars, *J. Fluid Mech.* **150**, pp.213-232, 1987.
10)Pornprommin, A. and Izumi, N., Nonlinear stability analysis of alternate and multiple bars, *2nd Proc. RCEM2001*, IAHR, Japan, pp.693-702, 2001.
11)Izumi, N. and Pornprommin, A., Weakly nonlinear analysis of bars with the use of the amplitude expansion method, *Proceedings of JSCE*, 2002. (in Japanese, accepted)
12)Egashira, S. and Takebayashi, H., Self-formed low water channel in straight channel, *1st Proc. RCEM1999*, IAHR, Italy, 1999.
13)Takebayashi, H., Egashira, S. and Okabe, T., Stream formation process between confining banks of straight wide channels, *2nd Proc. RCEM2001*, IAHR, Japan, pp.575-584, 2001.
14)Kurabayashi, H., Shimizu, Y. and Jang, C. L., Numerical calculation of bed deformation in braided stream, *2nd Proc. RCEM2001*, IAHR, Japan, pp.703-712, 2001.
15)Kurabayashi, H. and Shimizu, Y., Numerical calculation of bed deformation in braided stream with emerged mid-channel bars, *Annual J. Hydraul. Eng.* **46**, JSCE, pp.743-748, 2002. (in Japanese)
16)Tsujimoto, T., Kitamura, T. and Kishimoto, M., Numerical simulation of braching process of flood levee and hydraulics to support it, *Advances in River Eng.* **8**, JSCE, pp.31-36, 2002.
17)Ferziger, J. H. and Peirc, M., *Computational method for fluid dynamics*, Springer, 1997.
18)Rhie, C. M. and Chow, W. L., A numerical study of the turbulent flow past an isolated airfoil with trailing edge separation, *AIAA J.* **21**, pp.1525-1532, 1983.
19)Ashida, K. and Michiue, M., Studies on bed load transportation for nonuniform sediment and river bed variation, *Disaster prevention research institute annuals* **14B**, Kyoto, pp.259-273, 1971 (in Japanese)
20)Nakagawa, H., Tsujimoto, T. and Murakami, S., Non-equilibrium bed load along side bank, *Proc.3rd Int. Sym. River Sedimentation*., Jackson, Mississippi, USA, pp.1029-2065, 1986
21)Engelund, F., Flow and bed topography in channel beds, *J. Hyd. Div.*, ASCE, **100(11)**, pp.1631-1648, 1974.
22)Dey, A. K., Kitamura, T. and Tsujimoto, T., Perturbations along headcut and their effects on gully formation, *J. Hydraulic, Coastal and Env. Eng.* **677/II-55**, JSCE, pp.205-213, 2001.
23)Fujita, Y., Experimental study on the flow characteristic over alternating bar, *Annual J. Hydraul. Eng.* **24**, JSCE, pp.329-337, 1980. (in Japanese)

(2002年4月19日受付)